



Synthesis and in vivo evaluation of [¹¹C]tariquidar, a positron emission tomography radiotracer based on a third-generation P-glycoprotein inhibitor

Florian Bauer^{b,c,†}, Claudia Kuntner^{a,†}, Jens P. Bankstahl^d, Thomas Wanek^a, Marion Bankstahl^d, Johann Stanek^{a,c}, Severin Mairinger^{a,b,c}, Bernd Dörner^b, Wolfgang Löscher^d, Markus Müller^c, Thomas Erker^{b,*}, Oliver Langer^{a,c}

^a Molecular Medicine, AIT Austrian Institute of Technology GmbH, Seibersdorf, Austria

^b Department of Medicinal Chemistry, University of Vienna, Austria

^c Department of Clinical Pharmacology, Medical University of Vienna, Austria

^d Department of Pharmacology, Toxicology & Pharmacy, University of Veterinary Medicine Hanover, Germany

ARTICLE INFO

Article history:

Received 12 April 2010

Revised 10 June 2010

Accepted 16 June 2010

Available online 22 June 2010

Keywords:

PET

[¹¹C]tariquidar

P-glycoprotein

Breast cancer resistance protein

Blood-brain barrier

ABSTRACT

The aim of this study was to develop a positron emission tomography (PET) tracer based on the dual P-glycoprotein (P-gp) breast cancer resistance protein (BCRP) inhibitor tariquidar (**1**) to study the interaction of **1** with P-gp and BCRP in the blood–brain barrier (BBB) in vivo. *O*-Desmethyl-**1** was synthesized and reacted with [¹¹C]methyl triflate to afford [¹¹C]-**1**. Small-animal PET imaging of [¹¹C]-**1** was performed in naïve rats, before and after administration of unlabeled **1** (15 mg/kg, *n* = 3) or the dual P-gp/BCRP inhibitor elacridar (5 mg/kg, *n* = 2), as well as in wild-type, *Mdr1a/b*^(-/-), *Bcrp1*^(-/-) and *Mdr1a/b*^(-/-)*Bcrp1*^(-/-) mice (*n* = 3). In vitro autoradiography was performed with [¹¹C]-**1** using brain sections of all four mouse types, with and without co-incubation with unlabeled **1** or elacridar (1 μM). In PET experiments in rats, administration of unlabeled **1** or elacridar increased brain activity uptake by a factor of 3–4, whereas blood activity levels remained unchanged. In *Mdr1a/b*^(-/-), *Bcrp1*^(-/-) and *Mdr1a/b*^(-/-)*Bcrp1*^(-/-) mice, brain-to-blood ratios of activity at 25 min after tracer injection were 3.4, 1.8 and 14.5 times higher, respectively, as compared to wild-type animals. Autoradiography showed approximately 50% less [¹¹C]-**1** binding in transporter knockout mice compared to wild-type mice and significant displacement by unlabeled elacridar in wild-type and *Mdr1a/b*^(-/-) mouse brains. Our data suggest that [¹¹C]-**1** interacts specifically with P-gp and BCRP in the BBB. However, further investigations are needed to assess if [¹¹C]-**1** behaves in vivo as a transported or a non-transported inhibitor.

© 2010 Elsevier Ltd. All rights reserved.

1. Introduction

The ATP-binding cassette (ABC) transporter P-glycoprotein (P-gp, ABCB1) was initially discovered in the 1970s as an active efflux transporter involved in the multidrug resistance of cancer cells, and was the first drug efflux transporter to be detected in endothelial cells at the human blood–brain barrier (BBB).^{1,2} It has been suggested that P-gp serves as a general defense mechanism in the mammalian BBB, protecting the brain from intoxication by

potentially harmful lipophilic compounds from natural sources and other lipophilic xenobiotics that otherwise could penetrate the BBB by simple diffusion without any limitation.³ Regional over-activity of P-gp and related transporters in the BBB contributes to the phenomenon of drug resistance in neurological disorders, such as epilepsy and depression, by impeding therapeutically effective concentrations of central nervous system (CNS) drugs at their sites of action.³

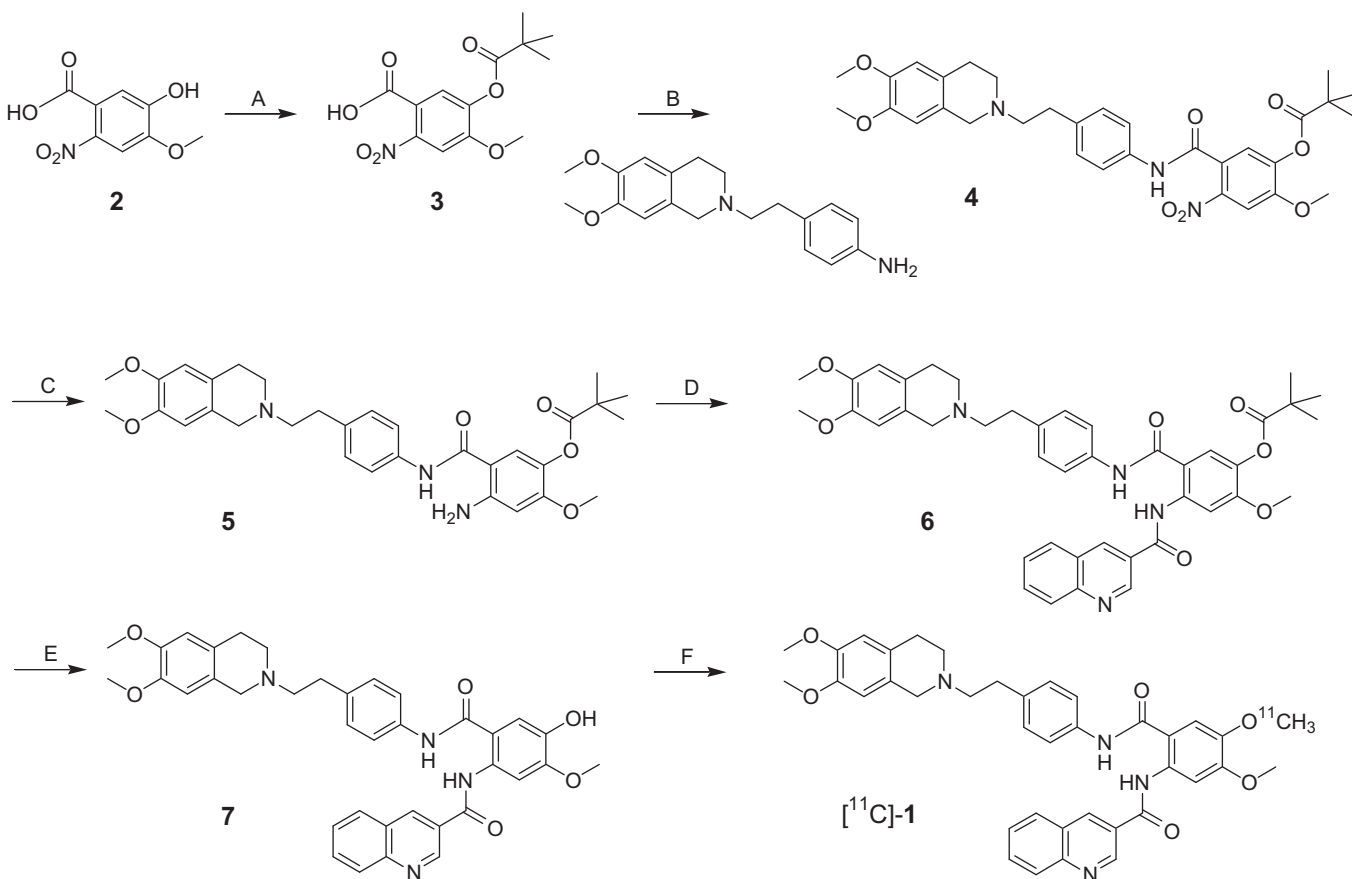
A promising strategy to enhance drug penetration across the BBB and thereby overcome drug resistance is the administration of third-generation P-gp inhibitors, which were originally developed as an adjunctive therapy for drug-resistant cancers and are characterized by a high potency in the nanomolar range, lack of toxicity and lack of cytochrome P450 interactions.⁴ The anthranilic acid derivative tariquidar (**1**, Scheme 1) is one of the most potent and selective third-generation P-gp inhibitors known to date.⁵ Unlike first- and second-generation P-gp inhibitors, such as verapamil, cyclosporine A or valsopodar (PSC 833), **1** is a non-competitive

Abbreviations: BBB, blood–brain barrier; BCRP, breast cancer resistance protein; *Bcrp1*^(-/-) mouse, BCRP knockout mouse; *Mdr1a/b*^(-/-) mouse, P-gp knockout mouse; *Mdr1a/b*^(-/-)*Bcrp1*^(-/-) mouse, P-gp/BCRP knockout mouse; PET, positron emission tomography; P-gp, P-glycoprotein; SPE, solid-phase extraction; SUV, standardized uptake value; TAC, time-activity curve.

* Corresponding author. Tel.: +43 1 4277 550 03; fax: +43 1 4277 9 551.

E-mail addresses: thomas.erker@univie.ac.at (T. Erker), oliver.langer@ait.ac.at (O. Langer).

† Florian Bauer and Claudia Kuntner contributed equally to this study.



Scheme 1. Synthesis of precursor **7** and its radiolabeling with [^{11}C]methyl triflate to give [^{11}C]-**1**. Reagents: (A) pivalic anhydride, DMF, Cs_2CO_3 ; (B) SOCl_2 , THF, Et_3N ; (C) H_2 , Pd/C, EtOAc/MeOH ; (D) 3-quinolinecarboxyl chloride, THF, Et_3N ; (E) NH_3 , EtOH , 50°C ; (F) [^{11}C]methyl triflate, aq NaOH, acetone, 60°C .

inhibitor and not a substrate of P-gp.⁶ Compound **1** also inhibits breast cancer resistance protein (BCRP, ABCG2), another ABC-type transporter expressed in the BBB, but at higher concentrations than those at which it inhibits P-gp.⁷ However, unlike first- and second-generation P-gp inhibitors, **1** does not inhibit multidrug resistance-associated proteins (MRPs), such as MRP1.⁸ Compound **1** was initially tested in clinical trials in cancer patients in combination with anticancer drugs that are P-gp substrates (e.g., paclitaxel, docetaxel, doxorubicin, vinorelbine), which demonstrated treatment response in some patients.⁵ However, some of these trials had to be discontinued because of increased toxicity of treatment regimens, which has been attributed to enhanced systemic exposure to anticancer drugs due to peripheral P-gp inhibition.^{4,5}

In contrast to its well-studied role in blocking P-gp in chemoresistant cancer cells, considerably less is known about the capacity of **1** to inhibit P-gp in the BBB and thereby facilitate brain entry of CNS drugs. A number of animal studies have shown that brain levels of antiepileptics, cytostatics and other CNS drugs were increased following administration of **1**.^{9–12} Only few human studies assessing the effect of **1** on P-gp in the BBB have been conducted to date. Kurnik et al. studied brain penetration of the P-gp substrate loperamide by measuring reduction in pupil diameter as a surrogate marker for central opioid effect, with and without co-administration of **1** at a dose of 2 mg/kg body weight.¹³ This study failed to demonstrate an effect of **1** on loperamide's central effects, whereas inhibition of P-gp in lymphocytes was >90%, suggesting that P-gp in the BBB is more resistant to inhibition as compared to peripheral P-gp.¹⁰ In a study recently conducted at our center, the effect of **1** (2 mg/kg) on brain penetration of the P-gp substrate

(*R*)-[^{11}C]verapamil was measured by PET imaging in healthy subjects.¹⁴ Our study showed a modest but significant ($+24 \pm 15\%$) increase in (*R*)-[^{11}C]verapamil brain distribution volume, which suggested that higher doses of **1** might be needed in the clinic in order to improve the clinical efficacy of CNS drugs in therapy-refractory patients. On the other hand, in rats comparable plasma levels of **1** to those achieved in humans in our study caused an increase of approximately +300% in (*R*)-[^{11}C]verapamil brain distribution volume, which points to pronounced species difference in tariquidar-induced P-gp inhibition.¹⁵ Another human study assessed the effect of different doses of **1** on brain penetration of the P-gp substrate radiotracer [^{11}C]-*N*-desmethyl-loperamide and found a fourfold increase in brain radioactivity uptake after 6 mg/kg of **1**.¹⁶

An alternative approach to using radiolabeled P-gp substrates, such as (*R*)-[^{11}C]verapamil,^{12,14} [^{11}C]-*N*-desmethyl-loperamide,^{17,18} or 6,7-dimethoxy-2-[3-(5-[^{11}C]methoxy-1,2,3,4-tetrahydronaphthalen-1-yl)-propyl]-1,2,3,4-tetrahydro-isoquinoline ([^{11}C]MC-266)¹⁹ for studying the interaction of **1** with P-gp at the BBB would be to perform PET experiments directly with radiolabeled **1**. Such a radiotracer might, for example, help to better understand species differences in tariquidar-induced P-gp inhibition as well as the differential sensitivity of cerebral and peripheral P-gp to inhibition. As opposed to P-gp substrate radiotracers, radiolabeled **1** is expected to bind to P-gp at the BBB without being transported by it and thereby allow mapping of the distribution of cerebral P-gp.

The aim of this study was to develop carbon-11-labeled **1** ([^{11}C]-**1**) as a PET tracer to directly study the interaction of **1** with P-gp and BCRP in vivo. Here, we report on the precursor synthesis, ^{11}C -labeling and small-animal PET evaluation of [^{11}C]-**1**.

2. Results

2.1. Chemistry and radiolabeling

The radiolabeling precursor of [^{11}C]-**1**, *O*-desmethyl-tariquidar (**7**), was synthesized as outlined in Scheme 1. Commercially available 4,5-dimethoxy-2-nitrobenzoic acid was first mono-demethylated using aq KOH to yield the corresponding 5-hydroxy derivative **2** (see Supplementary data).²⁰ Derivative **2** was then pivaloyl-protected to give compound **3** (see Supplementary data), which was transformed into its acid chloride and coupled with 6,7-dimethoxy-2-(4-aminophenethyl)-1,2,3,4-tetrahydroisoquinoline to afford compound **4**.^{21,22} The NO_2 group in **4** was reduced by catalytic hydrogenation to obtain the corresponding anthranilic acid derivative **5**, which was reacted with 3-quinolinecarbonyl chloride to afford *O*-pivaloyl-tariquidar (**6**). The pivaloyl protective group in **6** was removed by NH_3 in EtOH to give **7**. For ^{11}C -labeling, **7** was reacted with [^{11}C]methyl triflate in acetone containing aq NaOH. [^{11}C]-**1** ready for iv injection was obtained in a decay-corrected radiochemical yield of $5.4 \pm 3.0\%$ ($n = 45$), based on [^{11}C]CH $_4$, in a total synthesis time of approximately 40 min. Radiochemical purity was greater than 98% (see Supplementary data) and specific activity at end of synthesis was $114 \pm 67 \text{ GBq}/\mu\text{mol}$ ($n = 13$). The identity of [^{11}C]-**1** was confirmed by HPLC co-injection with unlabeled **1** (see Supplementary data).

2.2. Small-animal PET in rats and mice

[^{11}C]-**1** was evaluated in rats by performing paired PET scans: a baseline scan (scan 1) and a second scan after administration of unlabeled **1** or elacridar (scan 2) (Fig. 1). In scan 1, brain uptake of activity was low. Peak brain uptake was 0.71 ± 0.14 (standardized uptake value, SUV) at 0.5–1.3 min after tracer injection. At 25 min after tracer injection, brain activity uptake had declined to 0.19 ± 0.02 . In response to administration of unlabeled **1** (15 mg/kg) or elacridar (5 mg/kg) at 60 min after injection of [^{11}C]-**1** there was a steep increase in brain activity concentration, reaching SUVs of 0.43 ± 0.03 and 0.71 ± 0.06 , respectively, at 130 min after tracer injection, whereas blood activity levels appeared unchanged (Fig. 1). In scan 2, performed after injection of unlabeled **1** or elacridar, brain activity uptake at 25 min after tracer injection was 2.9 ± 0.8 and 4.3 ± 1.2 times higher as compared to scan 1, respectively, with similar blood activity levels as in scan 1 (Fig. 1). In Figure 2, representative PET summation images are shown for scans recorded before and after inhibitor administration.

Radiometabolites of [^{11}C]-**1** in plasma were assessed by a solid-phase extraction (SPE) assay. At 20 min after [^{11}C]-**1** injection, $4 \pm 4\%$ of total plasma activity was recovered in SPE fractions 1 and 2 (corresponding to polar radiometabolites of [^{11}C]-**1**) and $96 \pm 4\%$ in fraction 3 ($n = 8$, mean values of 20-min samples collected in scans 1 and 2). At 60 min after second [^{11}C]-**1** injection, $4 \pm 5\%$ of total plasma activity was in fractions 1 and 2, and $96 \pm 5\%$ in fraction 3. Fraction 3 was further analyzed by radio-high-performance liquid chromatography (HPLC), which suggested that unchanged [^{11}C]-**1** was the only radioactive species present, even though it cannot be excluded that radiometabolites of [^{11}C]-**1** were hidden under the broad HPLC peak of [^{11}C]-**1**. Representative HPLC chromatograms for samples collected at 20 and 60 min after tracer injection are shown in the Supplementary data.

In Figure 3, PET summation images and brain time-activity curves (TACs) of [^{11}C]-**1** in wild-type, *Mdr1a/b*^(-/-), *Bcrp1*^(-/-) and *Mdr1a/b*^(-/-)*Bcrp1*^(-/-) mice are shown. Brain TACs were higher in all transporter knockout mice as compared to wild-type animals (Fig. 3B). In *Mdr1a/b*^(-/-)*Bcrp1*^(-/-) mice, brain TACs were strikingly different as compared to the other three mouse types in that brain

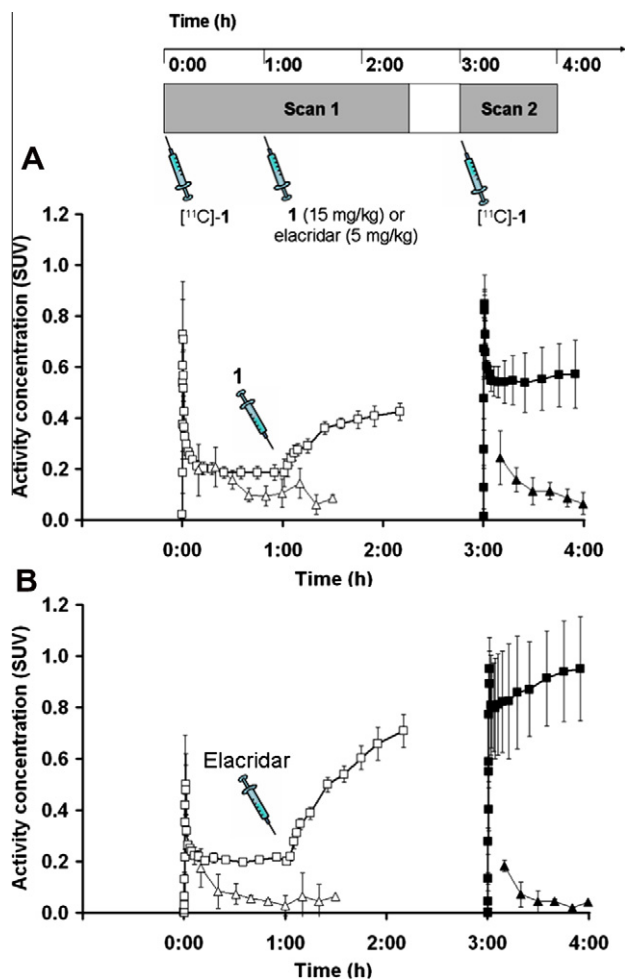


Figure 1. TACs (mean SUV \pm standard deviation, SD) in whole brain (scan 1: open squares, scan 2: filled squares) and arterial blood (scan 1: open triangles, scan 2: filled triangles) for paired PET scans in rats using (A) unlabeled **1** (15 mg/kg, $n = 3$) or (B) elacridar (5 mg/kg, $n = 2$) as inhibitor. Inhibitor was administered as an iv bolus at 60 min after start of scan 1 (see timeline above).

activity rose constantly throughout the scan duration. Brain activity uptake at 25 min after tracer injection was normalized to mean blood activity levels measured in separate groups of animals. Brain-to-blood ratios of activity at 25 min after tracer injection were 3.4 ($p = 0.0006$), 1.8 ($p = 0.0009$) and 14.5 times ($p = 0.0002$) higher in *Mdr1a/b*^(-/-), *Bcrp1*^(-/-) and *Mdr1a/b*^(-/-)*Bcrp1*^(-/-) mice, respectively, as compared to wild-type animals (brain-to-blood ratios, wild-type: 1.0 ± 0.1 ; *Mdr1a/b*^(-/-): 3.3 ± 0.4 ; *Bcrp1*^(-/-): 1.8 ± 0.1 ; *Mdr1a/b*^(-/-)*Bcrp1*^(-/-): 14.4 ± 1.7).

2.3. In vitro autoradiography

Figure 4 shows results from in vitro autoradiography of brain sections from all four mouse types, performed with [^{11}C]-**1** alone or with mixtures of [^{11}C]-**1** and unlabeled **1** or elacridar. Compared to wild-type mouse brain, mean binding of [^{11}C]-**1** was 49% ($p = 0.003$), 41% ($p = 0.006$) and 46% ($p = 0.001$) lower in *Mdr1a/b*^(-/-), *Bcrp1*^(-/-) and *Mdr1a/b*^(-/-)*Bcrp1*^(-/-) mouse brain, respectively (Fig. 4A and B). Co-incubation of [^{11}C]-**1** with unlabeled **1** significantly reduced binding of [^{11}C]-**1** to brain sections of all four mouse types (Fig. 4C). Co-incubation with elacridar, on the other hand, only caused significant reductions of [^{11}C]-**1** binding in wild-type and *Mdr1a/b*^(-/-) mouse brain (Fig. 4C).

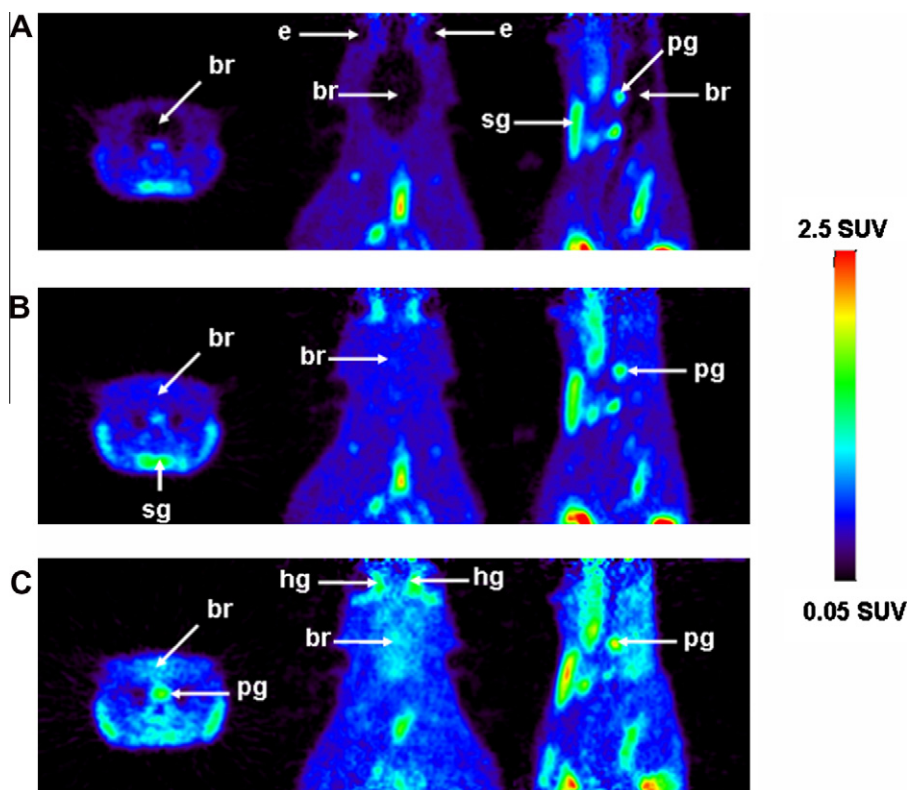


Figure 2. Exemplary coronal (left), horizontal (center) and sagittal (right) PET summation images in rats, (A) before administration of unlabeled inhibitor (scan 1: 0–60 min), (B) after administration of unlabeled **1** (15 mg/kg.), and (C) after administration of elacridar (5 mg/kg.). In (A) and (B) the same rat is shown. Activity concentration is expressed as SUV, and the radiation scale is set from 0.05 to 2.5. Anatomical structures are indicated by arrows (br, brain; e, eye; sg, submandibular gland; pg, pituitary gland; hg, haderian gland).

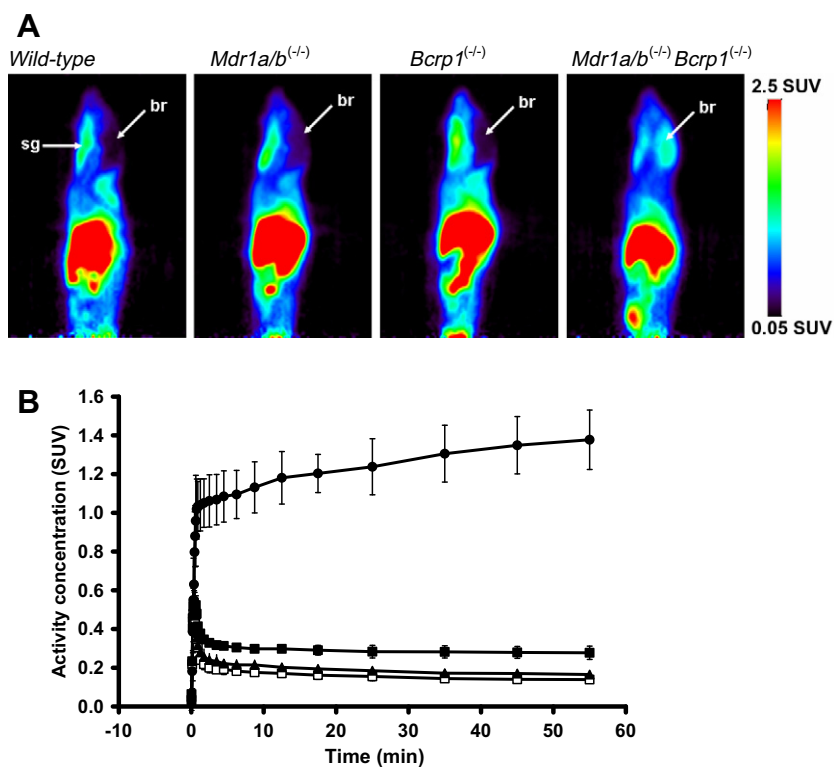


Figure 3. (A) Exemplary sagittal PET summation images (0–60 min) of wild-type, *Mdr1a/b*^(-/-), *Bcrp1*^(-/-) and *Mdr1a/b*^(-/-)*Bcrp1*^(-/-) mice. Activity concentration is expressed as SUV, and the radiation scale is set from 0.05 to 2.5. Anatomical structures are indicated by arrows (br, brain; sg, submandibular gland). (B) TACs (mean SUV ± SD, *n* = 3 per mouse type) in whole brain of wild-type (open squares), *Mdr1a/b*^(-/-) (filled squares), *Bcrp1*^(-/-) (filled triangles) and *Mdr1a/b*^(-/-)*Bcrp1*^(-/-) mice (filled circles).

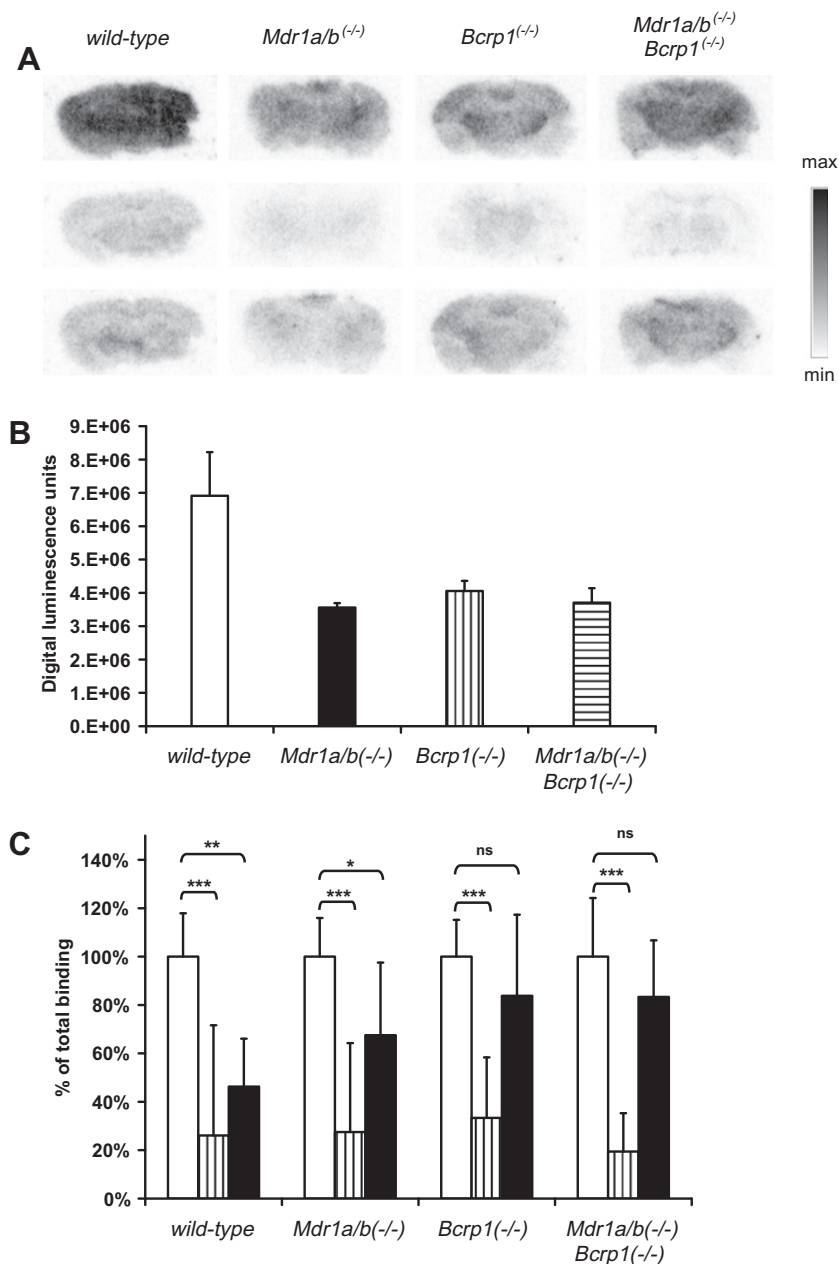


Figure 4. (A) In vitro autoradiograms of coronal brain slices (10 μm) of wild-type, *Mdr1a/b*^(-/-), *Bcrp1*^(-/-) and *Mdr1a/b*^(-/-)*Bcrp1*^(-/-) mice incubated with [¹¹C]-**1** alone (first row), with [¹¹C]-**1** and unlabeled **1** (1 μM, second row) and with [¹¹C]-**1** and unlabeled elacridar (1 μM, third row). (B) Binding of [¹¹C]-**1** to mouse brain sections (mean digital luminescence units ± SD) determined by in vitro autoradiography. (C) Displacement of [¹¹C]-**1** binding to mouse brain sections (mean ± SD) (white bars) by unlabeled **1** (hatched bars) or elacridar (black bars) (*, *p* < 0.05; **, *p* < 0.005; ***, *p* < 0.0005; ns, not significant; 2-tailed *t*-test).

3. Discussion

The aim of this study was to label **1** with a positron-emitting radionuclide and to assess the interaction of radiolabeled **1** with P-gp and BCRP in the BBB. As **1** contains four OCH₃ groups, the most straightforward radiolabeling approach was O-¹¹C-methylation of O-desmethyl-**1**, which offers the advantage that the radio-tracer retains the chemical structure of native **1** (Scheme 1). During the preparation of this manuscript a study by Kawamura et al. has appeared in the literature, which also reported on the ¹¹C-labeling of **1**, but in a different labeling position than in our work (i.e., on the dimethoxy-tetrahydroisoquinolinylethyl part of the molecule).²³ The in vivo specificity of [¹¹C]-**1** for P-gp and BCRP in the BBB was assessed by small-animal PET imaging using two

different approaches. First, we performed PET experiments in naïve rats before and after administration of unlabeled **1** or the potent dual P-gp/BCRP inhibitor elacridar. Second, we performed PET as well as in vitro autoradiography in wild-type mice and in *Mdr1a/b*^(-/-), *Bcrp1*^(-/-) and *Mdr1a/b*^(-/-)*Bcrp1*^(-/-) mice, which do not express the pharmacological targets of [¹¹C]-**1**.

3.1. Is [¹¹C]-**1** transported by P-gp?

Based on in vitro experiments with **1**, Mistry et al.⁸ first suggested that **1** is not transported by P-gp, which was substantiated by subsequent in vitro studies,^{6,24} indicating that **1** is a non-transported modulator of P-gp, which inhibits P-gp function by binding at a site that is distinct from the site(s) of interaction of transported substrates.^{6,25}

However, the in vivo behavior of [^{11}C]-**1** was comparable to what we had previously seen for the P-gp substrate (R)-[^{11}C]verapamil.^{12,15} In immediate response to injection of unlabeled **1** or elacridar, which was administered during [^{11}C]-**1** baseline PET scans in rats, brain activity started to rise significantly, with greater increases seen after administration of elacridar (Fig. 1B) than after **1** (Fig. 1A). In the second PET scan, performed after administration of unlabeled inhibitor, brain activity uptake was 3–4 times greater as compared to baseline scans (Figs. 1 and 2). Interestingly, similar results were obtained with [^{11}C]elacridar, another radiolabeled P-gp inhibitor developed in our laboratory.²⁶ Moreover, the P-gp inhibitor [^{11}C]laniquidar showed 6–9 times higher brain activity uptake after pretreatment with cyclosporine A (50 mg/kg, iv) in biodistribution studies in rats.²⁷ Also in transgenic mice, which lacked P-gp and/or BCRP, brain uptake of activity following injection of [^{11}C]-**1** was greater than in wild-type animals, which expressed both transporters in the BBB (Fig. 3).

Taken together, these observations may suggest that [^{11}C]-**1** behaves in vivo as a P-gp substrate rather than as a non-transported P-gp inhibitor. On the other hand, several lines of evidence suggest that **1** is a non-transported inhibitor of P-gp. According to Polli et al. the criteria for classifying a compound as a non-transported P-gp inhibitor are (i) a basolateral-apical (B-A) to apical-basolateral (A-B) concentration ratio <2 in monolayer transport assays, (ii) lack of adenosine triphosphatase activity stimulation and (iii) inhibition of substrate transport.²⁸ Compound **1** seems to meet all three criteria,^{6,24,25} but additional experiments with ^3H -labeled **1** might be warranted in the future to fully resolve this issue.

A possible explanation for the in vivo results obtained with [^{11}C]-**1** might be that a tracer dose of [^{11}C]-**1**, which contains <1 μg of unlabeled **1**, binds with nanomolar affinity (equilibrium dissociation constant K_D : 5.1 nM⁶) and a slow rate of dissociation to P-gp and possibly BCRP, which both act as gatekeepers at the BBB and thereby limit diffusion of [^{11}C]-**1** into brain.²⁶ Administration of unlabeled **1** or elacridar might have displaced [^{11}C]-**1** from its P-gp/BCRP binding site, resulting in unhindered passive diffusion of unmetabolized [^{11}C]-**1** from blood into brain. As brain activity levels rose above blood levels during the later part of scan 1 (Fig. 1), it can be assumed that diffusion into brain was driven by one or more so far unknown binding processes in brain, which were apparently not saturated at the administered doses of unlabeled **1** or elacridar. Displacement of P-gp binding of ^3H -labeled **1** by elacridar has been reported before.^{6,29} As elacridar and **1** appear to have distinct binding sites on P-gp, displacement of [^{11}C]-**1** binding by elacridar might have been caused by allosteric modulation.²⁹ Interestingly, we had previously seen only a weak increase in brain activity uptake during PET scans with [^{11}C]elacridar when unlabeled **1** was administered,²⁶ but this might be related to the fact that the employed dose of **1** (3 mg/kg) did not completely inhibit P-gp.¹⁵

In order to further substantiate our assumption of P-gp/BCRP-specific in vivo binding of [^{11}C]-**1**, in vitro autoradiography of mouse brain sections was performed with [^{11}C]-**1**. Importantly, brain sections of knockout mice, which lacked either P-gp or BCRP or both, showed approximately 50% less binding of [^{11}C]-**1** as compared to wild-type mouse brain (Fig. 4A and B). This is exactly the opposite of what we had seen in the in vivo experiments (Fig. 3), where knockout mice showed higher brain activity uptake than wild-type mice. As the BBB does not act as gatekeeper in the autoradiography setup lower binding of [^{11}C]-**1** in knockout mice most likely reflects the absence of P-gp and/or BCRP. Furthermore, the specificity of [^{11}C]-**1** binding to mouse brain sections was investigated by co-incubation with unlabeled **1** or elacridar. The dual P-gp/BCRP inhibitor elacridar was able to significantly displace [^{11}C]-**1** binding in mouse brain sections expressing P-gp and BCRP (wild-type mice), but not in brain sections of *Mdr1a/b*^(-/-)*Bcrp1*^(-/-) and *Bcrp1*^(-/-) mice (Fig. 4C). In *Mdr1a/b*^(-/-) mouse brain sections, significant displacement of

[^{11}C]-**1** binding by elacridar was seen, but it was clearly less pronounced than in wild-type mice. Unlabeled **1**, on the other hand, displaced [^{11}C]-**1** binding from all four types of mouse brain sections, apparently independent of the presence or absence of P-gp and/or BCRP. The reasons for this lack of differentiation of [^{11}C]-**1** displacement by unlabeled **1** in the four studied mouse types remain unclear at present but might suggest that [^{11}C]-**1** additionally binds to another saturable binding site in mouse brain tissue that is different from P-gp and BCRP. However, this site will probably be irrelevant for PET imaging due to the gatekeeper function of P-gp/BCRP. Our assumption that [^{11}C]-**1** binds to P-gp and is not transported by P-gp is further supported by pilot data acquired in a rat model of P-gp overexpression,³⁰ which revealed increased brain uptake of [^{11}C]-**1** as compared to naïve rats, whereas brain uptake of the P-gp substrate (R)-[^{11}C]verapamil was decreased.³¹

3.2. Does [^{11}C]-**1** selectively interact with P-gp in the BBB?

PET experiments in wild-type and *Mdr1a/b*^(-/-), *Bcrp1*^(-/-) and *Mdr1a/b*^(-/-)*Bcrp1*^(-/-) mice suggested that the contribution of P-gp to limiting brain entry of [^{11}C]-**1** was greater than the contribution of BCRP, as reflected by approximately two times higher brain-to-blood ratios of activity in *Mdr1a/b*^(-/-) compared to *Bcrp1*^(-/-) mice (Fig. 3). On the other hand, the combined effect of P-gp and BCRP knockout (*Mdr1a/b*^(-/-)*Bcrp1*^(-/-) mice) on brain uptake of [^{11}C]-**1** was far greater than the sum of its individual contributions in *Mdr1a/b*^(-/-) and *Bcrp1*^(-/-) mice. This observation has also been made by other investigators for other P-gp/BCRP substrate drugs^{23,32,33} and points to a concerted action of P-gp and BCRP in the BBB. In the absence of P-gp, BCRP may take over its role in limiting brain entry of dual substrates and vice versa. Moreover, it cannot be ruled out that *Mdr1a/b*^(-/-) mice, as a compensatory mechanism, show increased levels of BCRP in the BBB³⁴ and vice versa. Data from in vitro autoradiography suggested that [^{11}C]-**1** binds to both P-gp and BCRP, but were not able to discern the individual contributions of the two transporters to [^{11}C]-**1** binding.

3.3. Is [^{11}C]-**1** useful as a PET tracer for mapping the distribution of P-gp/BCRP at the BBB?

P-gp is a target protein which is ubiquitously and abundantly expressed in brain tissue. Kamiie et al. report a density (B_{max}) of the *Mdr1a* peptide of 15 fmol/ μg protein in mouse brain capillaries, which translates to a value of 75 nM when assuming a vascular volume in brain tissue of approximately 5% and a protein content of brain capillaries of approximately 10%.³⁵ The ratio of the B_{max} of a given target protein to the K_D of a prospective radioligand is commonly used as a predictor of the target-to-nontarget ratio to be expected for in vivo imaging.³⁶ Based on a K_D value for binding of tritiated **1** to Chinese hamster ovary resistant cells (CH 2 B30) of 5.1 nM,⁶ the B_{max}/K_D is approximately 15 for **1**, which should allow for obtaining a sufficiently high in vivo signal with [^{11}C]-**1**. Despite this B_{max}/K_D ratio, the PET signal obtained with [^{11}C]-**1** was low (brain uptake (SUV) 0.19 ± 0.02 at 25 min after tracer injection into rats), which might not be optimal for in vivo imaging and limit an accurate quantification of P-gp/BCRP expression levels with [^{11}C]-**1**.

We hypothesize that the low brain uptake of [^{11}C]-**1** might result from the gatekeeper function of P-gp/BCRP, which prevents brain entry of the radiolabeled probe, presumably by P-gp/BCRP-specific binding. A possible advantage of the gatekeeper function of P-gp/BCRP might be that it prevents non-specific binding of the highly lipophilic probe (log P 5.52) in brain tissue, which would mask P-gp/BCRP-specific binding. Looking at the brain TACs in *Mdr1a/b*^(-/-)*Bcrp1*^(-/-) mice (Fig. 3) gives a good impression of the high level of non-specific binding that would be obtained with [^{11}C]-**1** if it was not for the gatekeeper function of P-gp/BCRP.

If the small brain PET signal obtained with [^{11}C]-**1** is indeed specific to P-gp/BCRP in the BBB, the apparent lack of non-specific binding might therefore still make [^{11}C]-**1** useful for imaging transporter distribution at the BBB. Along the same lines, the apparently good metabolic stability of [^{11}C]-**1** (96% unchanged parent in plasma at 60 min after injection of [^{11}C]-**1** to rats) can be considered as an advantage, as radiometabolites of [^{11}C]-**1**, if present, might show P-gp/BCRP-independent brain uptake, such as is the case for (R)-[^{11}C]verapamil,³⁷ and thereby potentially contaminate the P-gp/BCRP-specific signal of [^{11}C]-**1**. The metabolic stability of [^{11}C]-**1**, at least in rodents, appears to be superior to that of most other P-gp PET probes ((R)-[^{11}C]verapamil, [^{11}C]-N-desmethyl-loperamide, [^{11}C]laniquidar, [^{11}C]elacridar).^{17,26,27,37}

Another important factor that comes into play when judging the utility of [^{11}C]-**1** for mapping cerebral P-gp is the possible influence of species differences. Previous data point to pronounced species differences in the P-gp system between rats and humans.^{15,38} We were able to show that comparable plasma concentrations of **1** had an effect about 10 times smaller on (R)-[^{11}C]verapamil brain distribution in humans as compared to rats, suggesting that P-gp expression is higher in the human BBB.^{14,15} This is also consistent with the observation that baseline brain distribution volume of (R)-[^{11}C]verapamil was two times lower in humans than in rats.^{14,15} This might in turn mean that [^{11}C]-**1**, which, based on *in vitro* experiments with unlabeled **1**, binds to P-gp and is not transported by it,^{6,8,24} will give a higher signal in humans than in rats.

4. Material and methods

4.1. General

All chemicals were purchased from Sigma-Aldrich Chemie GmbH (Schneidorf, Germany), Merck (Darmstadt, Germany) or Apollo Scientific Ltd (Bredbury, UK) at analytical grade and used without further purification. The dimesylate of **1** was obtained from Xenova Ltd (Slough, UK). The dual P-gp/BCRP inhibitor elacridar hydrochloride was obtained from Glaxo SmithKline (Research Triangle Park, NC, USA). For administration, **1** dimesylate was freshly dissolved on each experimental day in 2.5% (w/v) aqueous (aq) dextrose solution and injected at a volume of 3 mL/kg. Elacridar hydrochloride was dissolved in 20% aq EtOH and injected at a volume of 2 mL/kg. [^{11}C]CH₄ was produced via the $^{14}\text{N}(p,\alpha)^{11}\text{C}$ nuclear reaction by irradiating nitrogen gas containing 10% hydrogen using a PETtrace cyclotron equipped with a CH₄ target system (GE Healthcare, Uppsala, Sweden). [^{11}C]CH₃I was prepared in a TRACERlab FXC Pro synthesis module (GE Healthcare) and converted into [^{11}C]methyl triflate by passage through a column containing silver-triflate impregnated graphitized carbon.³⁹ ^1H and ^{13}C NMR spectra were recorded on a Bruker Advance DP × 200 (200 and 50 MHz). Chemical shifts are reported in δ units (ppm) relative to Me₄Si line as internal standard (s, bs, d, m, Cq for singlet, broad singlet, doublet, multiplet and quaternary carbon, respectively) and *J* values are reported in Hertz. Mass spectra (MS) were obtained with a Shimadzu (GC-17A; MS-QP5050A) spectrometer. Purity of compounds **4**, **5**, **6** and **7** was established by analytical HPLC confirming a purity >95%.

4.2. Animals

Adult female Sprague Dawley rats weighing 270–290 g were obtained from Harlan Netherlands (Horst, Netherlands). Female FVB (wild-type), *Mdr1a/b*^(-/-), *Bcrp1*^(-/-) and *Mdr1a/b*^(-/-)*Bcrp1*^(-/-) mice weighing 25–30 g were purchased from Taconic Inc. (Germantown, USA). The study was approved by the local Animal

Welfare Committee and all study procedures were performed in accordance with the Austrian Animal Experiments Act.

4.3. 5-(4-[2-(6,7-Dimethoxy-1,2,3,4-tetrahydro-2-isoquinolinyl)ethyl]anilinocarbonyl)-2-methoxy-4-nitrophenyl pivalate (**4**)

5-[(2,2-Dimethylpropanoyl)oxy]-4-methoxy-2-nitrobenzoic acid (**3**, 0.68 g, 2.29 mmol), which had been prepared from 5-hydroxy-4-methoxy-2-nitrobenzoic acid (**2**) as described in the [Supplementary data](#), was refluxed in SOCl₂ (4 mL) for 3 h. Excess SOCl₂ was evaporated. The acid chloride of **3** was dissolved in THF and slowly added to a solution of 6,7-dimethoxy-2-(4-aminophenethyl)-1,2,3,4-tetrahydroisoquinoline (0.68 g, 2.17 mmol) in THF containing Et₃N (1 mL), which had been prepared as described previously.²⁶ The reaction mixture was stirred overnight and then poured on ice H₂O. The precipitate was filtered off and dried to afford the title compound as a yellow solid (1.21 g, 94% theoretical yield).

MS *m/z* 590.60 (M–1, 0.05%), 206.15 (59.35%), 164.15 (43.98%), 57.15 (100%), 41.10 (32.77%). ^1H NMR (DMSO-*d*₆): δ 1.32 (s, 9H, CH₃), δ 2.64–2.82 (m, 8H), δ 3.56 (s, 2H, CH₂), δ 3.70 (s, 6H, OCH₃), δ 3.93 (s, 3H, OCH₃), δ 6.61–6.68 (m, 2H), δ 7.23 (d, 2H, *J* = 8.5 Hz), δ 7.56 (d, *J* = 8.5 Hz), δ 7.61 (s, 1H), δ 7.84 (s, 1H), δ 10.6 (s, 1H). ^{13}C NMR (DMSO-*d*₆): δ 26.7 (CH₃), δ 28.2 (CH₂), δ 32.4 (CH₂), δ 50.5 (CH₂), δ 55.0 (CH₂), δ 55.4 (OCH₃), δ 55.6 (OCH₃), δ 57.0 (OCH₃), δ 59.5 (CH₂), δ 108.9 (CH), δ 110.0 (CH), δ 111.8 (CH), δ 119.7 (CH), δ 123.5 (Cq), δ 125.8 (Cq), δ 126.5 (Cq), δ 128.9 (CH), δ 136.0 (Cq), δ 136.7 (Cq), δ 142.7 (Cq), δ 145.2 (Cq), δ 146.9 (Cq), δ 147.1 (Cq), δ 152.0 (Cq), δ 162.6 (CON), δ 175.1 (COO).

4.4. 4-Amino-5-(4-[2-(6,7-dimethoxy-1,2,3,4-tetrahydro-2-isoquinolinyl)ethyl]anilinocarbonyl)-2-methoxyphenyl pivalate (**5**)

To a solution of compound **4** (1.15 g, 1.94 mmol) in EtOAc/MeOH (1:1, 90 mL), which had been purged with argon, Pd/C catalyst (10%, w/w, 0.12 g) suspended in EtOAc/MeOH (1:1, 15 mL) was added. Hydrogen gas was introduced into the reaction mixture. The reaction mixture was stirred under normal pressure until hydrogen uptake was complete. The mixture was filtered and evaporated to give the title compound as a white solid (0.94 g, 86% theoretical yield).

MS *m/z* 561.30 (M⁺, 0.37%), 207.15 (15.76%), 206.15 (100%), 166.15 (10.91%), 57.10 (17.20%). ^1H NMR (DMSO-*d*₆): δ 1.29 (s, 9H, CH₃), δ 2.61–2.82 (m, 8H), δ 3.54 (s, 2H, CH₂), δ 2.68–2.74 (m, 9H, OCH₃), δ 6.41 (s, 1H), δ 6.59–6.71 (m, 4H), δ 7.19 (d, 2H, *J* = 8.4 Hz), δ 7.42 (s, 1H), δ 7.57 (d, 2H, *J* = 8.4 Hz), δ 9.72 (s, 1H). ^{13}C NMR (DMSO-*d*₆): δ 26.9 (CH₃), δ 28.3 (CH₂), δ 32.4 (CH₂), δ 50.6 (CH₂), δ 55.1 (CH₂), δ 55.4 (OCH₃), δ 55.5 (OCH₃), δ 55.5 (OCH₃), δ 59.6 (CH₂), δ 99.2 (CH), δ 105.5 (Cq), δ 110.0 (CH), δ 111.8 (CH), δ 120.8 (CH), δ 122.0 (CH), δ 125.9 (Cq), δ 126.6 (Cq), δ 128.5 (CH), δ 128.9 (Cq), δ 135.3 (Cq), δ 137.1 (Cq), δ 146.9 (Cq), δ 147.1 (Cq), δ 150.4 (Cq), δ 154.1 (Cq), δ 166.7 (CON), δ 176.3 (COO).

4.5. O-Pivaloyl-tariquidar (**6**)

3-Quinolinecarboxylic acid (0.26 g, 1.50 mmol) was refluxed in SOCl₂ (4 mL) for 3 h followed by evaporation of excess SOCl₂. The acid chloride was then suspended in THF and slowly added to a suspension of **5** (0.39 g, 0.69 mmol) in THF containing Et₃N (0.75 mL). The reaction mixture was stirred overnight and then poured on ice H₂O. The precipitate was filtered off and dried to

afford the title compound as an off-white solid (0.36 g, 72% theoretical yield).

HRMS (ESI/MS): calcd for $C_{42}H_{44}O_7N_4H$: 717.3288, found: 717.3285. 1H NMR (DMSO- d_6): δ 1.32 (s, 9H), δ 2.73–2.98 (m, 8H), δ 3.67 (s, 2H, CH_2), δ 3.82–3.87 (m, 6H, $2 \times OCH_3$), δ 3.90 (s, 3H, OCH_3), δ 6.55 (s, 1H), δ 6.61 (s, 1H), δ 7.24–7.32 (m, 2H), δ 7.40 (s, 1H), δ 7.56 (d, 2H, $J = 8.5$ Hz), δ 7.61–7.68 (m, 1H), δ 7.77–7.88 (m, 1H), δ 8.5 (d, 1H, $J = 8.2$ Hz), δ 8.30 (s, 1H), δ 8.72 (s, 1H), δ 8.74–8.79 (m, 1H), δ 9.49–9.55 (m, 1H), 12.77 (s, 1H, NH). ^{13}C NMR (DMSO- d_6): δ 26.6 (CH_3), δ 28.6 (CH_2), δ 33.4 (CH_2), δ 51.0 (CH_2), δ 55.6 (CH_2), δ 55.9 (OCH_3), δ 55.9 (OCH_3), δ 56.2 (OCH_3), δ 60.1 (CH_2), δ 105.2 (CH), δ 109.4 (CH), δ 111.3 (CH), δ 112.0 (Cq), δ 121.1 ($2 \times CH$), δ 121.3 (CH), δ 126.0 (Cq), δ 126.3 (Cq), δ 126.8 (Cq), δ 127.0 (Cq), δ 127.4 (CH), δ 129.2 (CH), δ 129.4 ($2 \times CH$), δ 131.5 (CH), δ 134.3 (Cq), δ 135.3 (Cq), δ 136.0 (CH), δ 137.3 (Cq), δ 140.3 (Cq), δ 147.2 (Cq), δ 148.7 (CH), δ 149.3 (Cq), δ 154.5 (Cq), δ 164.0 (CON), δ 166.7 (CON), δ 175.1 (COO).

4.6. O-Desmethyl-tariquidar (7)

Compound **6** (0.21 g, 0.29 mmol) was suspended in NH_3 (2 M in EtOH, 30 mL) and stirred at 50 °C for 24 h. The mixture was then evaporated and the product was purified by column chromatography (EtOAc/EtOH, 4:1) to afford the title compound as an off-white solid (0.10 g, 55% theoretical yield).

HRMS (ESI/MS): calcd for $C_{37}H_{36}N_4O_6H$: 633.2713, found: 633.2715. 1H NMR (DMSO- d_6): δ 2.58–2.91 (m, 8H), δ 3.53 (s, 2H, CH_2), δ 3.70 (s, 6H, OCH_3), δ 3.92 (s, 3H, OCH_3), δ 6.57–6.71 (m, 2H), δ 7.23 (d, 2H, $J = 8.5$ Hz), δ 7.44 (s, 1H), δ 7.60–7.76 (m, 3H), δ 7.86–7.98 (m, 1H), δ 8.10–8.18 (m, 2H), δ 8.21 (s, 1H), δ 8.84–8.92 (m, 1H), δ 9.23–9.46 (m, 2H), δ 10.32 (s, 1H), δ 12.14 (s, 1H). ^{13}C NMR (DMSO- d_6): δ 28.3 (CH_2), δ 32.4 (CH_2), δ 50.5 (CH_2), δ 55.1 (CH_2), δ 55.4 (OCH_3), δ 55.5 (OCH_3), δ 55.7 (OCH_3), δ 59.5 (CH_2), δ 105.5 (CH), δ 110.0 (CH), δ 111.7 (CH), δ 115.2 (Cq), δ 115.4 (CH), δ 121.0 (CH), δ 125.9 (Cq), δ 126.5 (Cq), δ 126.6 (Cq), δ 127.4 (CH), δ 127.5 (Cq), δ 127.6 (CH), δ 128.7 (CH), δ 129.3 (CH), δ 131.5 (CH), δ 132.1 (Cq), δ 135.5 (CH), δ 136.2 (Cq), δ 136.5 (Cq), δ 142.2 (Cq), δ 146.9 (Cq), δ 147.1 (Cq), δ 148.2 (CH), δ 148.6 (Cq), δ 150.3 (Cq), δ 162.8 (CON), δ 167.0 (CON).

4.7. [^{11}C]Tariquidar ([^{11}C]-1)

Using a TracerLab FXC Pro synthesis module, [^{11}C]methyl triflate was bubbled through a solution of **7** (0.3 mg, 0.47 μ mol) in acetone (0.5 mL) containing aq NaOH (0.3 M, 5 μ L, 1.5 μ mol, 3.2 equiv). After heating for 4 min at 60 °C, the reaction mixture was cooled (25 °C), diluted with H_2O (0.5 mL) and injected into a built-in HPLC system. A Chromolith Performance RP 18-e (100–4.6 mm) column (Merck KGaA, Darmstadt, Germany) was eluted at a flow rate of 5 mL/min with $CH_3CN/MeOH$ /ammonium acetate buffer (0.2 M, pH 5.0) (252:56:692, v/v/v). The HPLC eluate was monitored in series for radioactivity and ultraviolet (UV) absorption at a wavelength of 227 nm. On this system radiolabeling precursor **7** and product [^{11}C]-**1** eluted with retention times of 3 min and 6–8 min, respectively. The product fraction was diluted with H_2O (100 mL) and passed over a C18 Sep-Pak Plus cartridge (Waters Corporation, Milford, USA), which had been pre-activated with EtOH (5 mL) and H_2O (10 mL). The cartridge was then washed with H_2O (10 mL) followed by elution of [^{11}C]-**1** from the cartridge with EtOH (3 mL). The EtOH was then removed by heating at 100 °C under a stream of argon and the product formulated in a mixture of 0.9% aq saline/EtOH/polyethylene glycol 300 (50:15:35, v/v/v) at an approximate concentration of 370 MBq/mL for iv injection into animals. Radiochemical purity and specific activity of [^{11}C]-**1** was determined by analytical radio-HPLC using a Nucleosil 100–3 C18

column (3 μ m, 3.00 \times 125 mm, Macherey-Nagel, Düren, Germany) eluted with $CH_3CN/MeOH$ /ammonium acetate buffer (0.2 M, pH 5.0) (385:86:529, v/v/v) at a flow rate of 0.5 mL/min. UV detection was performed at a wavelength of 227 nm. The retention time of [^{11}C]-**1** was about 12–15 min on this HPLC system.

4.8. Small-animal PET imaging and PET data analysis

Prior to each experiment, the animals were placed into an induction box and anesthetized with 2.5% isoflurane. When unconscious, the animals were taken from the box and kept under anesthesia with 1.5–2% isoflurane administered via a mask during the whole experiment. The animals were warmed throughout the whole experiment at around 38 °C. Rats were implanted with catheters into the femoral artery (for blood sampling) and vein (for administration of [^{11}C]-**1** and unlabeled inhibitor). In mice, a lateral tail vein was used for radiotracer administration. The animals were positioned in the imaging chamber and [^{11}C]-**1** (rats: 97 ± 50 MBq in a volume of about 0.3 mL corresponding to 0.85 ± 0.44 nmol or 0.55 ± 0.28 μ g of unlabeled **1**; mice: 30 ± 8 MBq in a volume of about 0.1 mL corresponding to 0.26 ± 0.07 nmol or 0.17 ± 0.05 μ g of unlabeled **1**) was administered as an iv bolus over approximately 30 s. At the start of radiotracer injection, dynamic PET imaging was initiated using a microPET Focus220 scanner (Siemens, Medical Solutions, Knoxville, USA).

Rats underwent paired PET scans with [^{11}C]-**1**, before and after administration of unlabeled inhibitor (**1**, 15 mg/kg, $n = 3$, or elacridar, 5 mg/kg, $n = 2$) (see study outline in Fig. 1). Unlabeled inhibitor was injected iv over approximately 60 s at 60 min after start of scan 1, which was followed by a further 90 min of PET data acquisition. Scan 2 was performed at 2 h after injection of unlabeled inhibitor (Fig. 1). During experiments in rats, 5- μ L arterial blood samples were withdrawn manually with pre-weighted micropipettes from the femoral artery (approximately every 5 s) during the first 3 min after radiotracer injection, followed by further 10- μ L samples taken at 5, 10, 20, 30, 40, 50, 60, 70, 80 and 90 min (last three time points for scan 1 only). Moreover, one larger blood sample (0.6 mL) was collected into a heparinized vial at 20 min (scan 1 and scan 2) after tracer injection in order to determine metabolism of [^{11}C]-**1**. At the end of scan 2, the rats were sacrificed. A terminal blood sample (5 mL) was collected and radiometabolites of [^{11}C]-**1** in plasma were determined using a previously described SPE/HPLC assay.²⁶ For HPLC analysis, the same chromatographic conditions as described above for the semipreparative HPLC purification of [^{11}C]-**1** were used.

Mice ($n = 3$ per mouse type) underwent single 60-min PET scans with [^{11}C]-**1**. A separate group of animals ($n = 3$ per mouse type), which did not undergo PET scanning, was injected under isoflurane-anesthesia with [^{11}C]-**1** (7 ± 4 MBq corresponding to 0.06 ± 0.04 nmol or 0.04 ± 0.02 μ g of unlabeled **1**) for blood sampling. At 25 min after radiotracer injection, venous blood was withdrawn by retro-orbital puncture into pre-weighted micropipettes. Blood samples from the rats and mice were weighted and counted for activity in a 1-detector Wallac gamma counter (Perkin Elmer Instruments, Wellesley, USA), which had been cross-calibrated with the PET camera. Blood activity data were corrected for radioactive decay and corrected for injected dose per gram body weight and expressed as SUV.

PET images were reconstructed by Fourier rebinning followed by 2-dimensional filtered back projection with a ramp filter. The standard data correction protocol (normalization, attenuation, decay correction and injection decay correction) was applied to the data. Whole brain was manually outlined on multiple planes of the PET summation images using the image analysis software Amide and TACs, expressed as the SUV, were calculated. For the mouse data, the SUV values measured with PET in brain tissue of

individual animals at 25 min after radiotracer injection were divided by the mean SUV values in whole blood determined in the four separate groups of mice (see above) to obtain brain-to-blood ratios of activity.

For all outcome parameters, differences between groups were tested with a 2-tailed Student's *t*-test. The level of statistical significance was set to $p < 0.05$.

4.9. In vitro autoradiography

In vitro autoradiography of [¹¹C]-**1**, with and without co-incubation with unlabeled **1** or elacridar (1 μM), was carried out on brain sections (10 μm) of wild-type, *Mdr1a/b*^(-/-), *Bcrp1*^(-/-) and *Mdr1a/b*^(-/-)*Bcrp1*^(-/-) mice essentially as described elsewhere.²⁶

5. Conclusions

[¹¹C]-**1** was synthesized and a first in vivo evaluation performed using small-animal PET imaging. Our data suggest that [¹¹C]-**1** interacts specifically with P-gp and BCRP in the BBB. However, further experiments are needed to clarify if [¹¹C]-**1** behaves in vivo as a transported or as a non-transported P-gp/BCRP inhibitor.

Acknowledgments

The research leading to these results has received funding from the Austrian Science Fund (FWF) project 'Transmembrane Transporters in Health and Disease' (SFB F35) and from the European Community's Seventh Framework Programme (FP7/2007-2013) under grant agreement number 201380 ('Euripides'). The authors thank Gloria Stundner (AIT), Thomas Filip and Maria Zsebedics (Seibersdorf Laboratories GmbH) for their skillful help with laboratory animal handling. Elacridar hydrochloride was kindly provided by Glaxo SmithKline (Research Triangle Park, NC, USA) and the dimesylate of **1** by Xenova Ltd (Slough, UK).

Supplementary data

Supplementary data associated with this article can be found, in the online version, at doi:10.1016/j.bmc.2010.06.057.

References and notes

- Gottesman, M. M.; Ling, V. *FEBS Lett.* **2006**, *580*, 998.
- Miller, D. S.; Bauer, B.; Hartz, A. M. *Pharmacol. Rev.* **2008**, *60*, 196.
- Löscher, W.; Potschka, H. *Nat. Rev. Neurosci.* **2005**, *6*, 591.
- Szakacs, G.; Paterson, J. K.; Ludwig, J. A.; Booth-Genthe, C.; Gottesman, M. M. *Nat. Rev. Drug Disc.* **2006**, *5*, 219.
- Fox, E.; Bates, S. E. *Expert Rev. Anticancer Ther.* **2007**, *7*, 447.
- Martin, C.; Berridge, G.; Mistry, P.; Higgins, C.; Charlton, P.; Callaghan, R. *Br. J. Pharmacol.* **1999**, *128*, 403.
- Kühnle, M.; Egger, M.; Müller, C.; Mahringer, A.; Bernhardt, G.; Fricker, G.; König, B.; Buschauer, A. *J. Med. Chem.* **2009**, *52*, 1190.
- Mistry, P.; Stewart, A. J.; Dangerfield, W.; Okiji, S.; Liddle, C.; Bootle, D.; Plumb, J. A.; Templeton, D.; Charlton, P. *Cancer Res.* **2001**, *61*, 749.
- van Vliet, E. A.; van Schaik, R.; Edelbroek, P. M.; Redeker, S.; Aronica, E.; Wadman, W. J.; Marchi, N.; Vezzani, A.; Gorter, J. A. *Epilepsia* **2006**, *47*, 672.
- Choo, E. F.; Kurnik, D.; Muszkat, M.; Ohkubo, T.; Shay, S. D.; Higginbotham, J. N.; Glaeser, H.; Kim, R. B.; Wood, A. J.; Wilkinson, G. R. *J. Pharmacol. Exp. Ther.* **2006**, *317*, 1012.
- Hubensack, M.; Muller, C.; Hoehnerl, P.; Fellner, S.; Spruss, T.; Bernhardt, G.; Buschauer, A. *J. Cancer Res. Clin. Oncol.* **2008**, *134*(5), 597.
- Bankstahl, J. P.; Kuntner, C.; Abraham, A.; Karch, R.; Stanek, J.; Wanek, T.; Wadsak, W.; Kletter, K.; Müller, M.; Löscher, W.; Langer, O. *J. Nucl. Med.* **2008**, *49*, 1328.
- Kurnik, D.; Sofowora, G. G.; Donahue, J. P.; Nair, U. B.; Wilkinson, G. R.; Wood, A. J.; Muszkat, M. *Anesthesiology* **2008**, *109*, 1092.
- Wagner, C. C.; Bauer, M.; Karch, R.; Feurstein, T.; Kopp, S.; Chiba, P.; Kletter, K.; Löscher, W.; Müller, M.; Zeitlinger, M.; Langer, O. *J. Nucl. Med.* **2009**, *50*, 1954.
- Kuntner, C.; Bankstahl, J. P.; Bankstahl, M.; Stanek, J.; Wanek, T.; Stundner, G.; Karch, R.; Brauner, R.; Meier, M.; Ding, X. Q.; Müller, M.; Löscher, W.; Langer, O. *Eur. J. Nucl. Med. Mol. Imaging* **2010**, *37*, 942.
- Kreisl, W. C.; Liow, J. S.; Kimura, N.; Seneca, N.; Zoghbi, S. S.; Morse, C. L.; Herscovitch, P.; Pike, V. W.; Innis, R. B. *J. Nucl. Med.* **2010**, *51*, 559.
- Lazarova, N.; Zoghbi, S. S.; Hong, J.; Seneca, N.; Tuan, E.; Gladding, R. L.; Liow, J. S.; Taku, A.; Innis, R. B.; Pike, V. W. *J. Med. Chem.* **2008**, *51*, 6034.
- Liow, J. S.; Kreisl, W.; Zoghbi, S. S.; Lazarova, N.; Seneca, N.; Gladding, R. L.; Taku, A.; Herscovitch, P.; Pike, V. W.; Innis, R. B. *J. Nucl. Med.* **2009**, *50*, 108.
- van Waarde, A.; Ramakrishnan, N. K.; Rybczynska, A. A.; Elsinga, P. H.; Berardi, F.; de Jong, J. R.; Kwizera, C.; Perrone, R.; Cantore, M.; Sijbesma, J. W. A.; Dierckx, R. A.; Colabufio, N. A. *J. Med. Chem.* **2009**, *52*, 4524.
- Weber, C.; Bielak, A.; Demeter, A.; Borza, I.; Szendrei, G. I.; Keseru, G. M.; Greiner, I. *Tetrahedron* **2005**, *61*, 9375.
- Ashworth, P. A.; Hunjan, S.; Pretswell, I. A.; Ryder, H.; Brocchini, S. *J. PCT Int. Appl. WO 96/20180*, 1996.
- Sharp, M. J.; Mader, C. J.; Strachan, C. *PCT Int. Appl. WO 98/52923 A1*, 1998.
- Kawamura, K.; Konno, F.; Yui, J.; Yamasaki, T.; Hatori, A.; Yanamoto, K.; Wakizaka, H.; Takei, M.; Nengaki, N.; Fukumura, T.; Zhang, M. *R. Ann. Nucl. Med.* **2010**, *24*, 403.
- Rothnie, A.; Storm, J.; McMahon, R.; Taylor, A.; Kerr, I. D.; Callaghan, R. *FEBS Lett.* **2005**, *579*, 3984.
- Martin, C.; Berridge, G.; Mistry, P.; Higgins, C.; Charlton, P.; Callaghan, R. *Biochemistry* **2000**, *39*, 11901.
- Dörner, B.; Kuntner, C.; Bankstahl, J. P.; Bankstahl, M.; Stanek, J.; Wanek, T.; Stundner, G.; Mairinger, S.; Löscher, W.; Müller, M.; Langer, O.; Erker, T. *J. Med. Chem.* **2009**, *52*, 6073.
- Luurtsema, G.; Schuit, R. C.; Klok, R. P.; Verbeek, J.; Leysen, J. E.; Lammertsma, A. A.; Windhorst, A. D. *Nucl. Med. Biol.* **2009**, *36*, 643.
- Polli, J. W.; Wring, S. A.; Humphreys, J. E.; Huang, L.; Morgan, J. B.; Webster, L. O.; Serabjit-Singh, C. S. *J. Pharmacol. Exp. Ther.* **2001**, *299*, 620.
- Martin, C.; Berridge, G.; Higgins, C. F.; Mistry, P.; Charlton, P.; Callaghan, R. *Mol. Pharmacol.* **2000**, *58*, 624.
- Bankstahl, J. P.; Löscher, W. *Epilepsy Res.* **2008**, *82*, 70.
- Kuntner, C.; Bankstahl, J. P.; Bankstahl, M.; Stanek, J.; Wanek, T.; Dörner, B.; Bauer, F.; Mairinger, S.; Erker, T.; Müller, M.; Löscher, W.; Langer, O. *Nuklearmedizin* **2009**, *48*, A152.
- de Vries, N. A.; Zhao, J.; Kroon, E.; Buckle, T.; Beijnen, J. H.; van Tellingen, O. *Clin. Cancer Res.* **2007**, *13*, 6440.
- Polli, J. W.; Olson, K. L.; Chism, J. P.; John-Williams, L. S.; Yeager, R. L.; Woodard, S. M.; Otto, V.; Castellino, S.; Demby, V. E. *Drug Metab. Dispos.* **2009**, *37*, 439.
- Cisternino, S.; Mercier, C.; Bourasset, F.; Roux, F.; Scherrmann, J. M. *Cancer Res.* **2004**, *64*, 3296.
- Kamiie, J.; Ohtsuki, S.; Iwase, R.; Ohmine, K.; Katsukura, Y.; Yanai, K.; Sekine, Y.; Uchida, Y.; Ito, S.; Terasaki, T. *Pharm. Res.* **2008**, *25*, 1469.
- Eckelman, W. C.; Mathis, C. A. *Nucl. Med. Biol.* **2006**, *33*, 161.
- Luurtsema, G.; Molthoff, C. F.; Schuit, R. C.; Windhorst, A. D.; Lammertsma, A. A.; Franssen, E. J. *Nucl. Med. Biol.* **2005**, *32*, 87.
- Syvänen, S.; Lindhe, O.; Palmer, M.; Kornum, B. R.; Rahman, O.; Langstrom, B.; Knudsen, G. M.; Hammarlund-Udenaes, M. *Drug Metab. Dispos.* **2009**, *37*, 635.
- Jewett, D. M. *Appl. Radiat. Isot.* **1992**, *43*, 1383.